Improved Spatial Resolution in a Three-Dimensional Acoustic Medical Imaging System Based on a Hybrid Method Using a Synthetic Aperture Technique

Hirofumi TAKI and Toru SATO

Graduate School of Informatics, Kyoto University, Kyoto 606-8501, Japan

For an acoustic real-time three-dimensional (3-D) imaging system with high spatial resolution, we propose a system based on a hybrid method using a synthetic aperture technique. We can change the transmit point in this system; thus, the coherent integration of multiple receive signals from different transmit points improves spatial resolution using a synthetic aperture technique. In the case of a time resolution of 300 3-D images/s, the $-3\,\mathrm{dB}$ lateral resolution of the proposed system is 1.30 λ in the x–z section and 1.17 λ in the y–z section for a 0.07 m depth, where the lateral resolution is improved from 16 transmit and receive events. The number of elements can be reduced to about 1/7.5 of a dense two-dimensional (2-D) array of a digital beamforming imager having the same time and spatial resolution.   [DOI: 10.1143/JJAP.46.4827]

1. Introduction

A volumetric three-dimensional (3-D) real-time high-resolution acoustic imaging system is needed for medical diagnosis. Since the 1960s, numerical image reconstruction using synthetic aperture techniques has been proposed.[1,2] Numerical image reconstruction utilizing the mechanical scanning of a single element is the simplest of these techniques.[3,4] A monostatic data acquisition scheme can be used to reconstruct images with an adequate spatial resolution. However, an imager using this method has an insufficient time resolution for practical clinical application.

A 3-D imager that employs a linear array measures one target plane at a time, and then moves mechanically[5–9] or freehand[10] for 3-D imaging. However, these methods, particularly the freehand scanning method, have an insufficient time resolution for the medical examination of a fast-moving organ such as the heart. Furthermore, the use of acoustic lenses on the elements to focus the transmit and receive beams to a target plane results in serious deterioration in spatial resolution both in front of and behind the focus.

One strategy for decreasing the number of elements, at a cost of the loss of some lateral resolution and signal-to-noise ratio (SNR), is to utilize a two-dimensional (2-D) sparse array with an element spacing of more than one-half of a wavelength. Turnbull and Foster[11] investigated the arrangement of such a sparse random 2-D array. Because the 2-D random array has no periodicity, the problem of grating lobes can be avoided. In addition, Sumanaweera et al. investigated 2-D spiral arrays.[12] Smith et al.[13] proposed the idea of using different transmit and receive geometries. Because a transmit beam and a receive beam have different radiation patterns, the directions of grating lobes become different. As a result, the grating lobe levels can be suppressed. This idea was developed by Lockwood and coworkers.[14,15] Austeng and Holm[16] investigated and made a comparative study of sparse arrays. Although several designs of sparse arrays have been reported, it is difficult to reduce the number of elements to less than one-half of that of dense arrays. Furthermore, a 3-D imager of this type has a low time resolution.

A digital beamforming imager that incorporates a 2-D array enables the measurement of the entire target field as a single transmit and receive event. This system, therefore, has a high time resolution; however, the number of elements on the 2-D array is enormous and the SNR is low.[17–19] An encoded wave front is utilized to improve time resolution and SNR.[20,21] This method needs linearity of the received signal; thus, the method is not useful for medical imaging with a poor linearity and a large dynamic range. Although a myocardial motion imager is useful for medical diagnoses,[22] it has an insufficient lateral resolution.

For the diagnoses of fatal heart diseases, we proposed a system based on a hybrid array-refrector configuration, as shown in Fig. 1.[23–25] This system employs a wide transmit beam that is radiated over the entire measurement field. The angular resolution and SNR of the proposed method are improvements over those of a digital beamforming imager with a similarly sized 2-D array. This is because in the current method most of the echo reflected by the mirror is gathered to the array.

In this paper, we propose a method for the improvement of the spatial resolution of a 3-D acoustic medical imaging
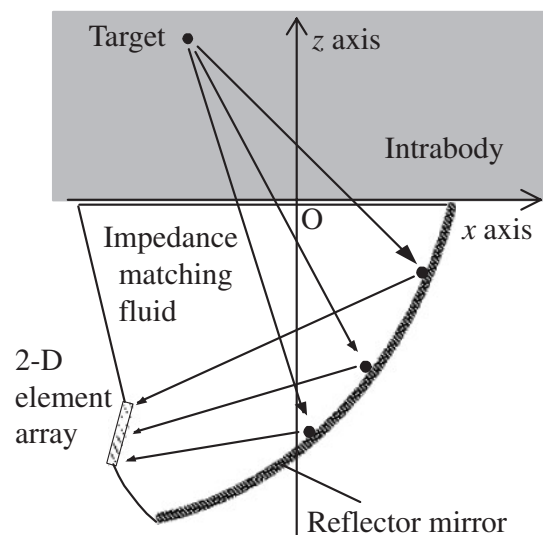

Fig. 1.   Schematic view of the system in the receive phase.

system based on a hybrid method that uses a synthetic aperture technique. Because a 3-D imager based on a hybrid method aquires a 3-D image as single transmit and receive event, the image reconstruction from multiple transmit and receive events realizes a sufficient time resolution for measuring a fast-moving organ such as the heart.

In §2, we outline the framework of the 3-D acoustic imaging system based on the hybrid method. We provide some necessary wave equations and parameters for calculating spatial resolution in §3. In the proposed imager, all elements on the 2-D array radiate ultrasound pulses at appropriate time delays for synthesizing a wide transmit beam. In §4, we propose a method to employ appropriate time delays. The radiation pattern of the transmit beam is calculated in §5. In §6, we evaluate the effect of the coherent integration of multiple transmit and receive events on the improvements in spatial resolution obtained in the proposed method. In §7, we examine the spatial resolution of the proposed imager in the case that the time resolution is 300 3-D images/s. Finally, we draw conclusions.

2. Formation of the Transmit Beam Using a Focusing Method

With this method, a transmit beam is radiated over the entire measurement field before any echoes from the targets are received on the 2-D array. The image of a target is reconstructed from the received signals using numerical back-projection. The image reconstruction based on numerical back-projection is processed as follows: the phase of the received signal is reversed before being projected backward from the receive point. The waves projected backward are focused at the target points.

To measure the entire target field as a single transmit and receive event, the transmit beam must be radiated sufficiently widely over the target field. Moreover, a high transmit power is desirable to improve the SNR. A method to form a wide transmit beam is shown in ref. 25. Figure 2 is a schematic view of the proposed imager in the transmit phase. All the elements on the array radiate ultrasound pulses at appropriate time delays to enable the pulses to be focused by the reflector. As a single element response placed at the focus is synthesized, a wide transmit beam with a high acoustic power is radiated over the entire target field.

3. Calculation of Acoustic Propagation

We calculated acoustic propagation for investigating the spatial resolution of a 3-D acoustic imager based on a hybrid method, as previously described.[25] Figure 3 shows the coordinate system for the calculation of received signals on the 2-D element array. All the elements radiate acoustic
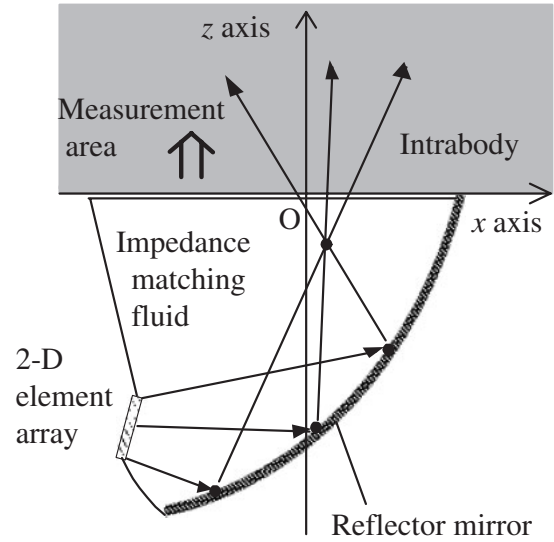

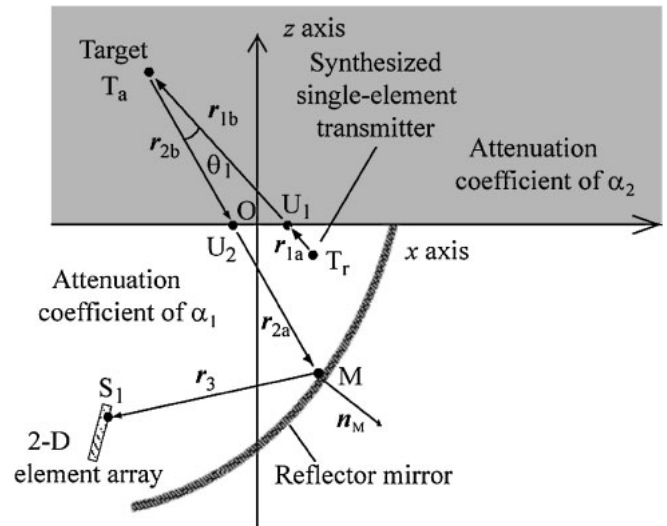Fig. 2. Schematic view of the system in the transmit phase.

Fig. 3. Arrangement of a 2-D element array and a mirror in a transmit and receive event.

pulses with appropriate time delays, and then the pulses are reflected on the mirror and focused at T_r. A broad beam is then radiated from this focus. The transmit beam is scattered at T_a by the inhomogeneity of the target. The backscattered echo is reflected on the mirror at M, and received by an element at S_1. U_1 and U_2 are the intersections of lines $T_r T_a$ and $T_a M$, respectively, in the x–y plane.

The received signal on the element at S_1 is given by

$$P_{S_1}(t) \propto \sum P_{1S_1}\{t - (r_{1a} + r_{1b} + r_{2a} + r_{2b} + r_3)/c_0\}\left\{\frac{\Delta c}{c_0} + (1 + \cos\theta_1)\frac{\Delta\rho}{2\rho_0}\right\}\frac{r_{2a}\cdot n_M}{r_{2a}n_M}\frac{\Delta S}{(r_{1a} + r_{1b})(r_{2a} + r_{2b})r_3}, \quad (1)$$

$$P_{1S_1}(t) = F^{-1}[-jk^3 e^{-\alpha_1(r_{1a}+r_{0b}+r_{0c})-\alpha_2(r_{1b}+r_{0a})}A(\omega)\Delta V/(8\pi^3)], \quad (2)$$

where $r_{1a} = \overrightarrow{T_r U_1}$, $r_{1b} = \overrightarrow{U_1 T_a}$, $r_{2a} = \overrightarrow{U_2 M}$, $r_{2b} = \overrightarrow{T_a U_2}$, $r_3 = \overrightarrow{MS_1}$, $r_{1a} = |r_{1a}|$, $r_{1b} = |r_{1b}|$, $r_{2a} = |r_{2a}|$, $r_{2b} = |r_{2b}|$, $r_3 = |r_3|$, $r_{0a} = |\overrightarrow{T_a O}|$, $r_{0b} = |\overrightarrow{OM_0}|$, $r_{0c} = |\overrightarrow{U_2 M}|$, ρ_0 is the density

of the undisturbed medium, c_0 is the mean propagation velocity, $\Delta\rho$ is the variation of the density, Δc is the variation of the propagation velocity, ω is the angular frequency, $k = \omega/c_0$ is the wave number, $\theta_1 = \angle T_r T_a M$, ΔV
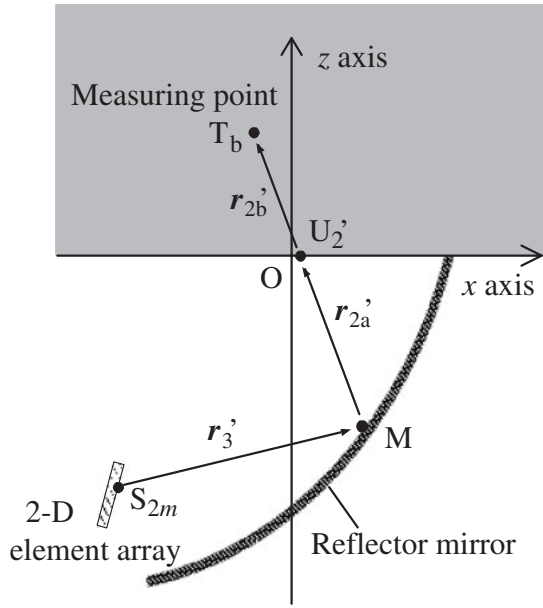
Fig. 4.   Arrangement of a 2-D element array and a mirror in the numerical back-projection.

Fig. 5.   Transmit waveform used in this study.

is the volume of a target, $A(\omega)$ is the frequency spectrum of the transmit beam radiated from T_r, $\boldsymbol{n}_M$ is the vector perpendicular to the mirror at M, $n_M = |\boldsymbol{n}_M|$, and ΔS is the square measure of the small area on the mirror. α_1 and α_2 are the attenuation coefficients of the impedance matching fluid and the intrabody, respectively.

We reconstructed images of targets from the distributed images on the array by numerical back-projection, as previously described.[22] Similar to the calculation of the received signal, we define an element and the measurement point existing respectively at S_{2m} and T_b, as shown in Fig. 4. The estimated power at T_b, the objective function, is given by

$$W_{T_b}(t)' \propto P_{T_b}(t)' P_{T_b}(t)'^*, \tag{3}$$

$$P_{T_b}(t)' = \sum P_{1T_b}\{t - (r_{2a}' + r_{2b}' + r_3')/c_0\}'$$
$$\times \frac{\boldsymbol{r_3}' \cdot \boldsymbol{n}_M}{r_3' n_M} \frac{\Delta S}{(r_{2a}' + r_{2b}')r_3'}, \tag{4}$$

$$P_{1T_b}(t)' = F^{-1}[-k^2 e^{-\alpha_1(r_{0b}+r_{0c})-\alpha_2 r_{0a}} p_m(\omega)'^*/(4\pi^2)], \tag{5}$$

where $\boldsymbol{r_{2a}}' = \overrightarrow{MU_2'}$, $\boldsymbol{r_{2b}}' = \overrightarrow{U_2'T_b}$, $\boldsymbol{r_3}' = \overrightarrow{S_{2m}M}$, $r_{2a}' = |\boldsymbol{r_{2a}}'|$, $r_{2b}' = |\boldsymbol{r_{2b}}'|$, $r_3' = |\boldsymbol{r_3}'|$, $p_m(\omega)'$ is the Fourier transform of the received signal on the element at S_{2m}. $p_{T_b}(t)'^*$ and $p_m(\omega)'^*$ are the complex conjugates of $p_{T_b}(t)'$ and $p_m(\omega)'$, respectively.

We set calculation parameters as follows: the mean propagation velocity $c_0 = 1600$ m/s, the density of the undisturbed medium $\rho_0 = 1.08 \times 10^3$ kg/m³, the variation of the propagation velocity $\Delta c = -300$ m/s, and the variation of the density $\Delta \rho = -1.0 \times 10^2$ kg/m³. α_1 and α_2 are $2.0(\omega/2\pi)^2 \times 10^{-14}$ and $5.0(\omega/2\pi) \times 10^{-6}$ Np/m, respectively. Figure 5 shows the transmit waveform used in the calculation of the spatial resolution, where the center frequency is 1.6 MHz and -6 dB fractional band width is 60%. The element pitch is one-half the wavelength λ at the center frequency, that is, the element pitch is 0.0005 m. Many researchers have investigated 2-D arrays with 500 to 1000 elements;[14,15] thus, we employ a circular 2-D array of 0.016 m in diameter, where the number of elements is 797,
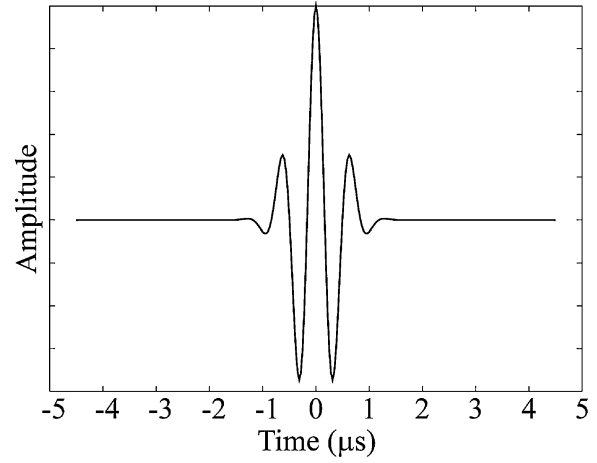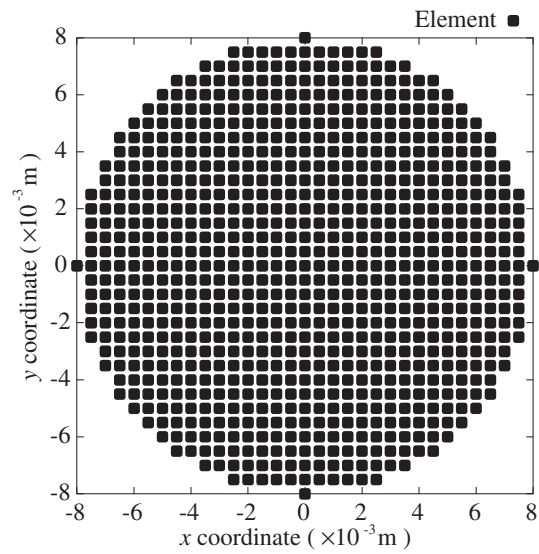

Fig. 6.   Element pattern for a 797-element array.

as shown in Fig. 6. Figure 7 shows the front view of the proposed imager. The reflector size is 0.062 m long and 0.08 m wide.

4.   Transmit Time Delays for Focusing the Transmit Beam

In this section, we first propose a method that utilizes numerical back-projection to calculate the transmit waveform for focusing the transmit pulses at a point. In this case, we assume that a spherical wave is radiated backward from the focus; we then calculate the received signal at each element on the array. The phase of the transmit pulse is the reverse of the received signal.

The waveform of the received signal is unique to each element because the transmission pass from the focus is unique to the element position. As radiating different individual waveforms from all elements is impractical because the number of elements is 797, all elements radiate ultrasound pulses of the same waveform with different time delays. We introduce the assumption that the waveform radiated backward from the focus is the same as that radiated from all elements. We calculate the time delay by maximizing

Jpn. J. Appl. Phys., Vol. 46, No. 7B (2007)
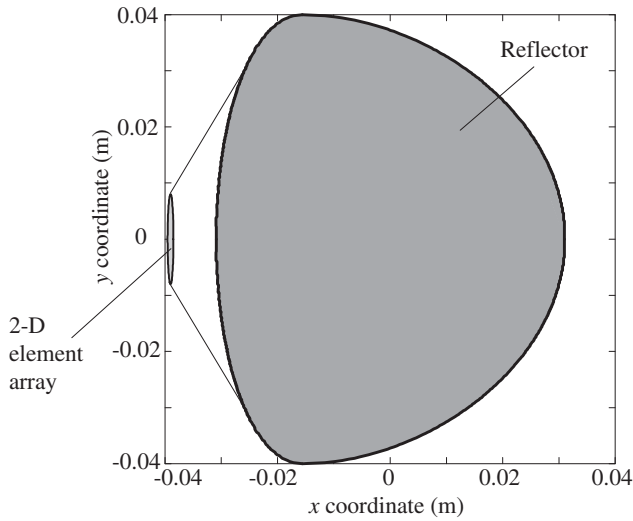
H. TAKI and T. SATO

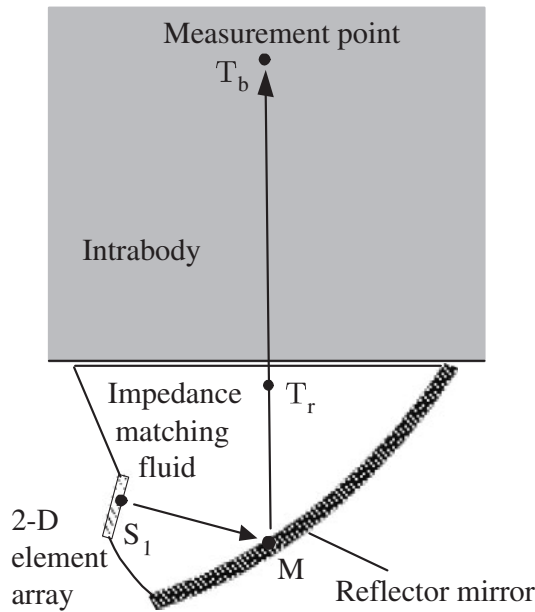Fig. 7. Front view of the proposed imager.

Fig. 8. Transmit pass in geometric optics. In geometric optics a transmit pulse from an element is reflected by the mirror, and then radiated to the measurement point T_b after passing through the focus T_r.

$$E(\tau) = \int p(t - \tau)q(t)\,dt, \tag{6}$$

where $p(t)$ is the waveform radiated backward from the focus, $q(t)$ is the waveform received at an element, and t is the transmit time delay of the element. The transmit waveform radiated from the element is $p(t + \tau)$.

5. Region with a Guaranteed Focus

In this section we evaluate the region in which the focus is guaranteed to radiate an ultrasound beam in a direction. In the geometric optics shown in Fig. 8, a transmit pulse from an element is reflected by the mirror and then radiated to the measurement point (T_b) after passing through the focus (T_r). Similarly, the inverse pass T_bT_r arrives at the array after being reflected by the mirror. To radiate a transmit beam to T_b, it is therefore necessary that the focus exists in the region
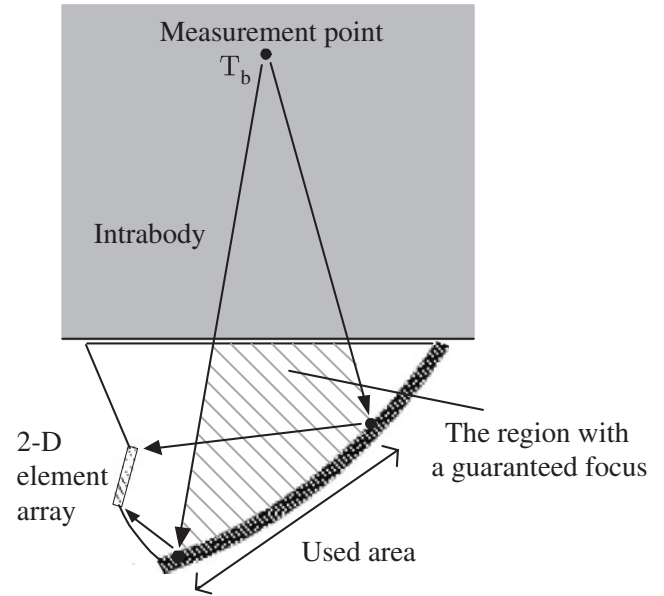

Fig. 9. Region with a guaranteed focus. When the focus is contained within the region, the transmit wave is radiated to the measurement point T_b.

between T_b and the used area. The used area is the region on the mirror where the echo from T_b is reflected and arrives at the array. We call this as the region with a guaranteed focus (RGF), as shown in Fig. 9.

Because the echo reflected by the used area on the mirror is received by the 2-D array, the proposed imager has a high SNR. The SNR improvement of the proposed imager, as compared with an imager without a reflector is given by

$$\text{SNR}_H = 10\log(R_H D) \text{ (dB)}, \tag{7}$$
$$R_H = A_H / A_{DBF}, \tag{8}$$

where A_H is the visual angle of the used area from the target, A_{DBF} is that of a 2-D array placed at the center of the x–z plane, and D is caused by the attenuation through the impedance matching fluid at the transmit and receive phases.[22] When the impedance matching fluids are water and ultrasound jelly, the SNR improvements SNR_H are 7.8 and 6.7 dB, respectively.

Figure 10 shows the radiation pattern of the proposed imager in the x–z section for (a) 0 and (b) 0.07 m depths. In this calculation we set the focus at the origin. The -6 dB transmit beam width is $1.8\,\lambda$ in the x–y section. This indicates that the transmit power is gathered at the focus; that is, the time delays employed for the elements are appropriate. At a 0.07 m depth in a region with an x coordinate more than -0.013 m and less than 0.03 m, the transmit power is greater than -6 dB, as compared with the peak power: the amplitude half-width is 33.7°. Therefore, the proposed imager measures a target field of 33.7° of the visual angle as a single transmit and receive event.

The radiation pattern of a transmit beam varies as the position of the focus. The proposed imager reconstructs a 3-D image from multiple transmit and receive events of various focal positions; thus, ultrasound is radiated to a target field wider than that when utilizing a single transmit and receive event. This indicates that the proposed imager utilizing multiple transmit and receive events can measure a
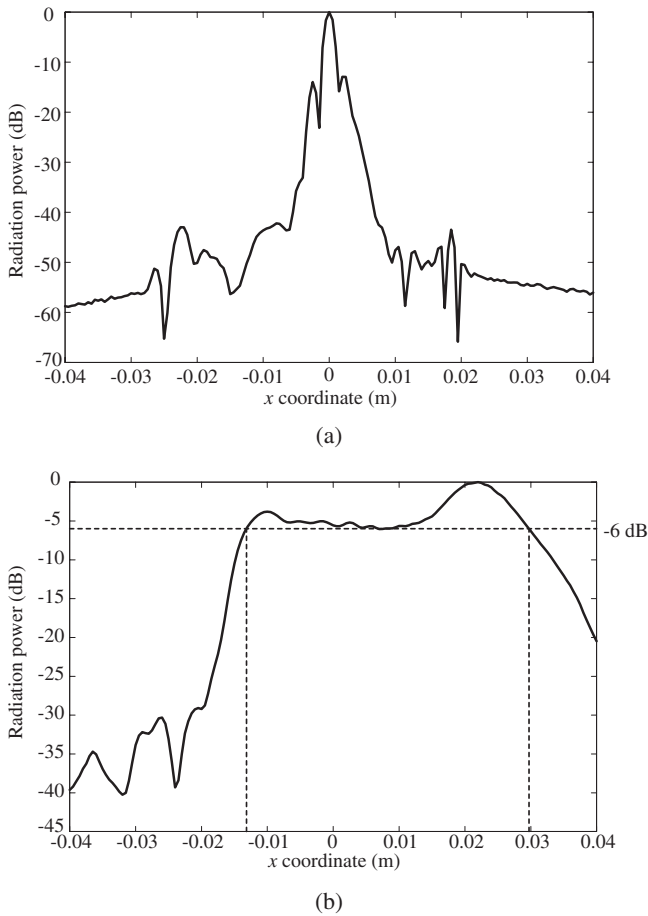
(a)

(b)

Fig. 10. Radiation pattern of the proposed imager in the x–z section for (a) 0 m and (b) 0.07 m depths. The focus is set at the origin.
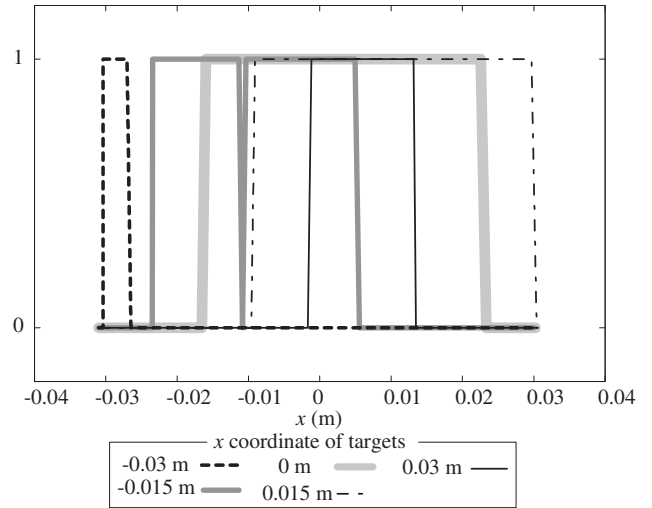

Fig. 11. Regions with a guaranteed focus on the x axis. The regions, whose x coordinates of measurement points are from -0.015 to 0.03 m, contain the origin, and that whose x coordinate is -0.03 m does not contain the origin. This corresponds to the radiation pattern shown in Fig. 10(b).
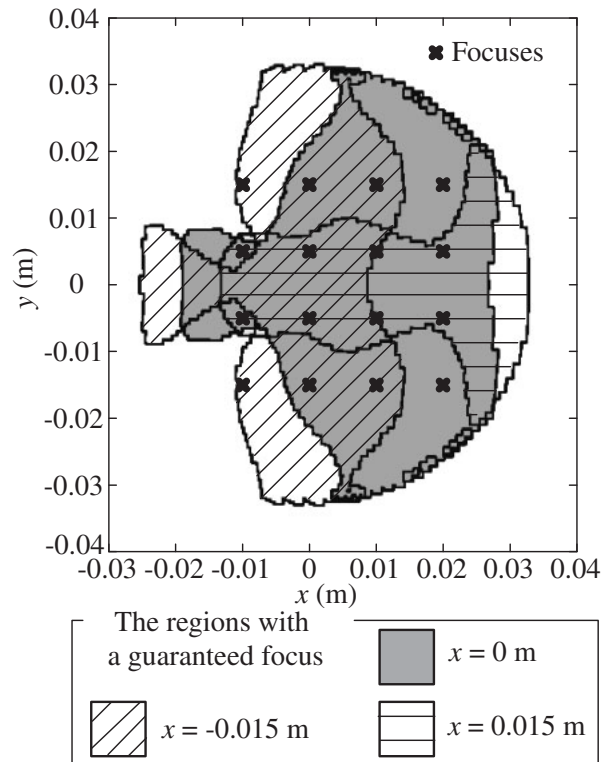

Fig. 12. Arrangement of the focuses and the regions with a guaranteed focus for a -0.01 m depth. The RGFs of the measurement points of $x = -0.015$, 0, and 0.015 m contain 10, 14, and 8 focuses, respectively.

target field of more than $33.7°$ of the visual angle. Therefore, the imager has a sufficient measurement field for the diagnoses of fetal heart diseases.

Figure 11 shows the RGFs on the x axis. The regions, whose x coordinates of measurement points are from -0.015 to 0.03 m, contain the origin, and that whose x coordinate is -0.03 m does not contain the origin. Because the transmit wave is radiated in the direction where the RGF contains the focus, the arrangement of RGFs shown in Fig. 11 corresponds to the radiation pattern shown in Fig. 10. Therefore, to radiate a certain measurement point, the focus should be arranged in the RGF of the point.

6. Improvement of Spatial Resolution by Multiple Transmit and Receive Events

Because a single transmit and receive event can generate a 3-D image using the proposed method, the time resolution is 5000 images/s when the measurement range is 0.16 m. For medical diagnoses, a lower time resolution is sufficient; therefore, spatial resolution and SNR can be improved from multiple transmit and receive events. Utilizing a synthetic aperture technique, the coherent integration of multiple receive signals of different transmit points equivalently increases aperture size; thus, the spatial resolution is improved. With this method, we can change the focal position by employing appropriate time delays.

When measuring a fast-moving organ, such as the heart of a fetus, a time resolution of 300 3-D images/s is required. In

this case, the spatial resolution can be improved from 16 transmit and receive events by using a synthetic aperture technique. To prevent burning of the skin, we arranged the 16 focuses for a -0.01 m depth, as shown in Fig. 12. The transmit wave is radiated in the direction where the RGF contains the focus. Therefore, the spatial resolutions for point targets at the x coordinates of -0.015, 0, 0.015 m are improved respectively from 10, 14, 8 transmit and receive events. Receiving a large part of the echo reflected on the
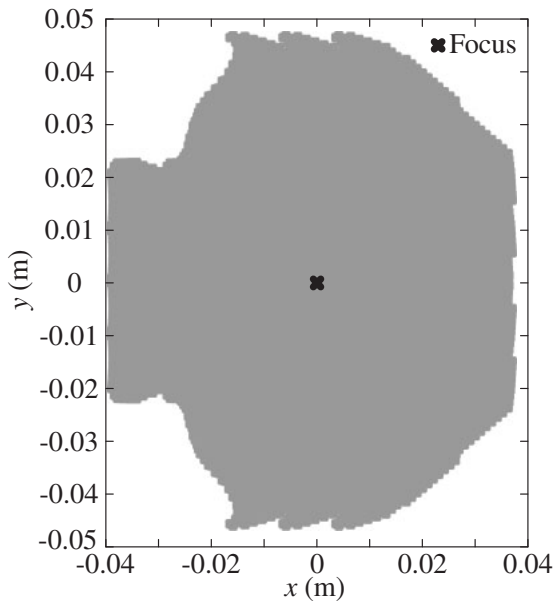
Fig. 13. Synthesized aperture from 14 transmit and receive events when measuring the center for a 0.07 m depth. The synthesized aperture is larger than a section of RGF; thus, the spatial resolution is improved utilizing the synthetic aperture technique.

Fig. 14. Range resolution of the proposed imager at the center. Two point targets are placed for 0.06 and 0.07 m depths, and the resolution is acquired from a single transmit and receive event. The lines show the estimated power at the measurement points.

Fig. 15. Lateral resolution of the proposed imager acquired from single and 16 transmit and receive events in the x–z section for a 0.07 m depth. A point target is placed at $x = -0.015$, 0, and 0.015 m in the x–z plane for a 0.07 m depth. The lines show the estimated power at the measurement points.

mirror has the same effect as using a large array. As shown in Fig. 9, the echo passing through a section of the RGF are received on the array; thus, the spatial resolution of the proposed imager is equivalent to that of a digital beamforming imager with an array of the same size as the section of the RGF. Therefore, we call the section of the RGF as the effective aperture. Figure 13 shows the synthesized aperture from 14 events when measuring the center for a 0.07 m depth, where we introduce the approximation that a spherical wave is radiated from the focus. The coherent integration utilizing the synthetic aperture technique realizes a spatial resolution equivalent to that of an aperture given by the convolution of the focuses and the effective aperture.

7. Results and Discussion

Figure 14 shows the range resolution of the proposed imager at the center. Two point targets are placed for 0.06 and 0.07 m depths, and the resolution is acquired from a single transmit and receive event. In this calculation we introduce the Born approximation. This indicates that the proposed imager has a sufficient range resolution.

Figure 15 shows the spatial resolution of the proposed imager acquired from a single and 16 transmit and receive events. As noted above, the spatial resolutions of the x coordinates of -0.015, 0, 0.015 m are improved, respectively, from 10, 14, 8 transmit and receive events, utilizing a synthetic aperture technique. This shows the effectiveness of the synthetic aperture technique for the lateral resolution improvement of the proposed imager.

We compare the spatial resolution of the proposed imaging method with that of the digital beamforming method. The spatial resolution of digital beamforming imagers is improved from 16 transmit and receive events. As shown in Fig. 16, the x–z and y–z section -3 dB lateral resolutions are about 1.30 λ and 1.17 λ, respectively. A target exists at the center for a 0.07 m depth. They are the
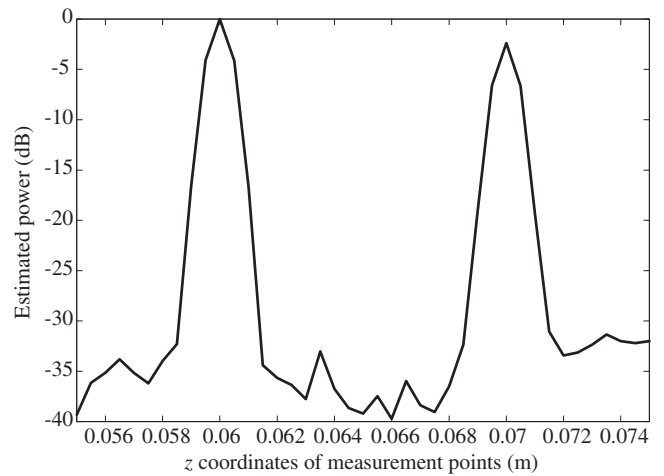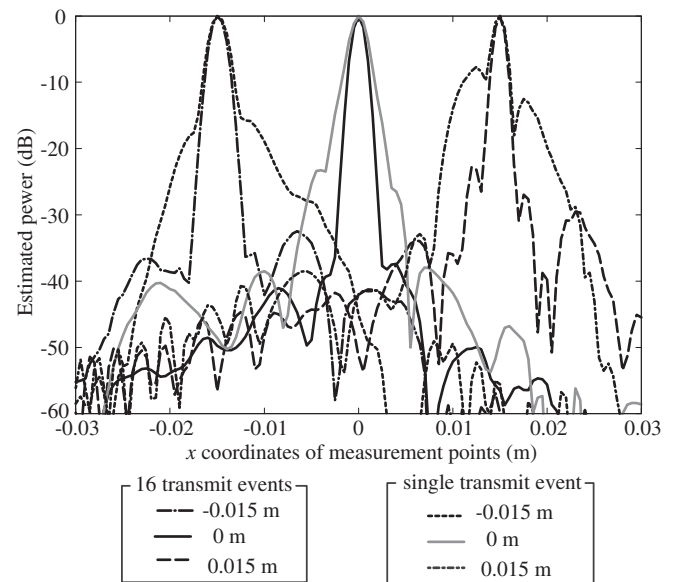
same as those of a digital beamforming imager with an elliptic array of 0.041 m long and 0.047 m wide. Because the elements are spaced at intervals of one-half of a wavelength on the array, the area of the array is proportional to the number of elements. Therefore, the number of elements can be reduced to about 1/7.5 of a dense 2-D array having the same spatial resolution.

8. Conclusions

To realize a high resolution acoustic real-time 3-D imaging system, we proposed a system based on a hybrid method utilizing a synthetic aperture technique. Because images of the entire measurement field are reconstructed as a single transmit and receive event, we can reconstruct a 3-D image from multiple transmit and receive events with a
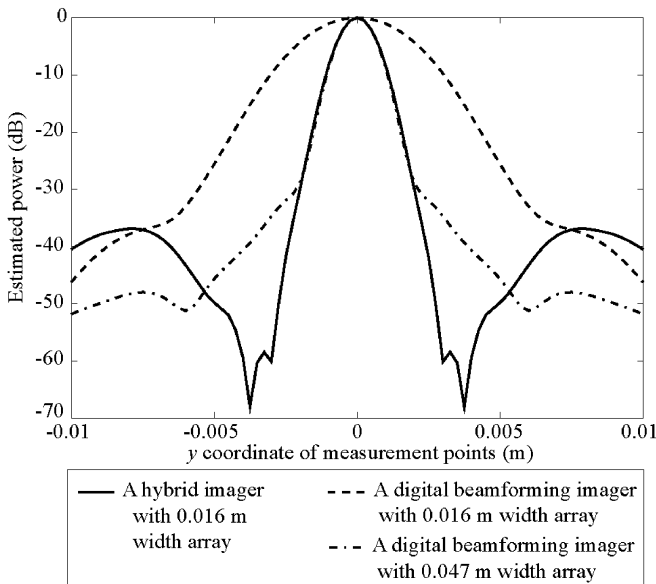
Fig. 16.   Lateral resolution of the proposed imager with a 0.016 m width array and digital beamforming imagers with 0.016 and 0.047 m width arrays. A point target exists at the center for a 0.07 m depth, and lines show the estimated power at the measurement points in the y–z section. The spatial resolutions of the proposed imager and digital beamforming imagers are improved, respectively, from 14 and 16 transmit and receive events.

sufficient time resolution. When the time resolution is 300 3-D images/s, the coherent integration of 16 transmit and receive events improves the spatial resolution utilizing the synthetic aperture technique. Image reconstruction from 16 events realizes a lateral resolution of 1.30 λ in the x–z section and 1.17 λ in the y–z section for a 0.07 m depth, where the center frequency is 1.6 MHz, the width of the reflector is 0.062 m long and 0.08 m wide, and the array is a circle 0.016 m in diameter. This shows that the number of elements can be reduced to about 1/7.5 of a dense 2-D array having the same spatial and time resolutions but using a digital beamforming method with a synthetic aperture technique.

1) J. J. Flaherty, K. R. Erikson, and V. M. Lund: U.S. Patent 3 548 642 (1967).
2) J. W. Goodman: in *Acoustical Holography*, ed. A. F. Metherell *et al.* (Plenum, New York, 1969) Vol. 1, 173.
3) J. T. Ylitalo and H. Ermert: IEEE Trans. Ultrason. Ferroelectr. Freq. Control **41** (1994) 333.
4) Z. M. Benenson, A. B. Elizarov, T. V. Yakovleva, and W. D. O'Brien, Jr.: IEEE Trans. Ultrason. Ferroelectr. Freq. Control **49** (2002) 1665.
5) B. Delannoy, R. Torguet, C. Bruneel, E. Bridous, J. M. Rouvaen, and H. LaSota: J. Appl. Phys. **50** (1979) 3153.
6) D. P. Shattuck, M. D. Weinshenker, S. W. Smith, and O. T. von Ramm: J. Acoust. Soc. Am. **75** (1984) 1273.
7) O. T. von Ramm, S. W. Smith, and H. G. Pavy, Jr.: IEEE Trans. Ultrason. Ferroelectr. Freq. Control **38** (1991) 109.
8) M. Karaman, P. C. Li, and M. O'Donnell: IEEE Trans. Ultrason. Ferroelectr. Freq. Control **42** (1995) 429.
9) G. R. Lookwood, J. R. Talman, and S. S. Brunke: IEEE Trans. Ultrason. Ferroelectr. Freq. Control **45** (1998) 980.
10) K. Kohyama, Y. Yasumuro, M. Imura, Y. Manabe, O. Oshiro, K. Moroi, and K. Chihara: Jpn. J. Appl. Phys. **44** (2005) 4637.
11) D. H. Turnbull and F. S. Foster: IEEE Trans. Ultrason. Ferroelectr. Freq. Control **38** (1991) 320.
12) T. S. Sumanaweera, J. Schwartz, and D. Napolitano: Proc. IEEE Int. Ultrasonics Symp., 1999, p. 1271.
13) S. W. Smith, H. G. Pavey, and O. T. Ramm: IEEE Trans. Ultrason. Ferroelectr. Freq. Control **38** (1991) 100.
14) G. R. Lookwood, P.-C. Li, and M. O'Donnell, *et al.*: IEEE Trans. Ultrason. Ferroelectr. Freq. Control **43** (1996) 7.
15) G. R. Lookwood and F. S. Foster: IEEE Trans. Ultrason. Ferroelectr. Freq. Control **43** (1996) 15.
16) A. Austeng and S. Holm: IEEE Trans. Ultrason. Ferroelectr. Freq. Control **49** (2002) 1073.
17) R. M. Lutolf, A. Vieli, and S. Basler: IEEE Trans. Ultrason. Ferroelectr. Freq. Control **36** (1989) 494.
18) B. D. Steinberg: IEEE Trans. Ultrason. Ferroelectr. Freq. Control **39** (1992) 716.
19) M. Karaman, P. C. Li, and M. O'Donnell: IEEE Trans. Ultrason. Ferroelectr. Freq. Control **42** (1995) 429.
20) S. Ishigami, H. Yanagida, Y. Tamura, C. Ishihara, and N. Okada: Jpn. J. Appl. Phys. **42** (2003) 3276.
21) N. Okada, M. Sato, C. Ishihara, N. Ishii, T. Aoki, T. Hisamoto, H. Yanagida, and Y. Tamura: Jpn. J. Appl. Phys. **42** (2003) 3289.
22) H. Kanai, H. Hasegawa, and K. Imamura: Jpn. J. Appl. Phys. **45** (2006) 4718.
23) H. Taki and T. Sato: Cho-onpa Igaku **33** (2006) S280 [in Japanese].
24) H. Taki and T. Sato: IEICE Tech. Rep., US106-109 (2006) [in Japanese].
25) H. Taki and T. Sato: to be published in J. Med. Ultrason.